

Article

Effects of Top Ceramic Layers with an Ultrathin Dense Layer on the Thermal–Physical Properties of Thermal Barrier Coatings

Li Ai ¹, Xueying Wang ², Ming Yang ^{3,*}, Yuntao Lei ¹ and Yongping Zhu ^{2,*}

¹ Beijing Power Machinery Research Institute, Beijing 100074, China; lai010105@163.com (L.A.); taoleiy@163.com (Y.L.)

² State Key Laboratory of Multi-Phase Complex Systems, Institute of Process Engineering, Chinese Academy of Sciences, Beijing 100190, China; xywang@ipe.ac.cn

³ School of Material Science and Engineering, Hubei Polytechnic University, Huangshi 435003, China

* Correspondence: yangming@hbpu.edu.cn (M.Y.); ypzhu@ipe.ac.cn (Y.Z.)

Abstract: Thermal barrier coatings have been used to protect superalloys under extremely harsh conditions. The durability of TBCs with a NiCoCrAlY bond layer prepared via the air plasma spray process and an ultrathin dense layer prepared via magnetron sputtering was investigated under different corrosion conditions. This paper discusses the corrosion resistance improvement mechanism of TBCs with a dense layer produced by magnetron sputtering under corrosion conditions with environmental contaminants such as calcium–magnesium–aluminum–silicon oxide systems (CMAS) at 1300 °C and NaCl–Na₂SO₄–V₂O₅ (NV) at 900 °C. The corrosion results show that CMAS will react with the stabilizers of zirconium oxide, which will change the rate of the phase transition, as determined via X-ray diffraction tests. A thermal ablation test verified that TBCs with a dense layer have a better corrosion resistance and better thermal insulation properties. All results show that preparing TBCs with a dense layer via the magnetron sputtering method will be an efficient method to improve TBCs' properties at high temperatures in the future.

Keywords: thermal barrier coatings; corrosion; oxygen permeation; air plasma spray; thermal insulation



Citation: Ai, L.; Wang, X.; Yang, M.; Lei, Y.; Zhu, Y. Effects of Top Ceramic Layers with an Ultrathin Dense Layer on the Thermal–Physical Properties of Thermal Barrier Coatings. *Coatings* **2023**, *13*, 1929. <https://doi.org/10.3390/coatings13111929>

Academic Editor: Angela De Bonis

Received: 11 October 2023

Revised: 30 October 2023

Accepted: 9 November 2023

Published: 11 November 2023



Copyright: © 2023 by the authors. Licensee MDPI, Basel, Switzerland. This article is an open access article distributed under the terms and conditions of the Creative Commons Attribution (CC BY) license (<https://creativecommons.org/licenses/by/4.0/>).

1. Introduction

Thermal barrier coatings (TBCs) were developed as a kind of thermal protection technology for some ceramic materials, with a high temperature stability, a low thermal conductivity, a high thermal expansion coefficient and corrosion resistance, and were designed to bind with metal substrates to form a coating to prolong the working time of metal substrates [1–7]. TBCs are mainly made from a ceramic top layer, a NiCoCrAlY bond layer and a superalloy substrate [8]. The most popular ceramic top layer material is yttria-stabilized zirconia (YSZ), which cannot work for a long time above 1200 °C as it will fail due to a phase transformation and oxidation of the bonding layer [3,9]. When oxygen infiltrates the metal bonding layer through the ceramic layer, the metal layer can be oxidized to form a thermally grown oxide (TGO) layer [10,11]. Furthermore, NaVO₃ and CaO + MgO + Al₂O₃ + SiO₂ (CMAS) corrosion will also accelerate the failure of TBCs during operation [12,13]. When CMAS reacts with stabilizers, it can produce a tetragonal to monoclinic phase transformation, which may occur upon cooling, accompanied by a 3%–5% volume expansion and a loss of coating toughness [14]. The oxygen to oxidize the TGO layer mainly comes from two places: one is the oxygen contained in TBCs during the spray process, and the other is the oxygen from the environment, which will infiltrate the top ceramic layer and enter the bonding layer at high temperatures. The large influx of oxygen will accelerate the oxidation of the metal bonding layer and increase the rate of formation of the TGO layer. Due to the difference in the thermal expansion coefficients of the TGO layer and the ceramic layer, a concentrated thermal stress area will be generated between the ceramic and metal bonding layers [15,16]. As the regional stress increases, the

ceramic layer and the metal bonding layer will peel off, ultimately causing the thermal barrier coating to fail.

To solve this problem, much research has been performed to prolong the working time of TBCs. Li [17] found that the chemical reaction between wet CMAS melts and YSZ is more vigorous on the YSZ (110) lattice surface than that on other interfaces from first principles calculations. Hamide [18] found that the hot corrosion mechanism involves molten salts reacting with the stabilizers of zirconia. Shen [19] studied the thermal shock life and failure behaviors of $\text{La}_2\text{Zr}_2\text{O}_7/\text{YSZ}$, $\text{La}_2\text{Ce}_2\text{O}_7/\text{YSZ}$ and $\text{Gd}_2\text{Zr}_2\text{O}_7/\text{YSZ}$ double-layer ceramic TBCs, and found that $\text{Gd}_2\text{Zr}_2\text{O}_7/\text{YSZ}$ TBCs have the longest thermal shock life. Wang [20] found that the high-entropy rare earth aluminate $(\text{Y}_{0.2}\text{Yb}_{0.2}\text{Lu}_{0.2}\text{Eu}_{0.2}\text{Er}_{0.2})_3\text{Al}_5\text{O}_{12}$ was stable at 1400 °C. Tounsi [21] employed an efficient and simple four-variable integral high-order shear deformation theory to model the analytical solution of the boundary condition. Katea [22] found that the obtained nano-particle TBCs might be of interest for high-temperature and harsh-environment applications. Doleker [23] studied TGO layers, finding that they are predominantly composed of an alumina layer at 1000 and 1100 °C; however, an increase in mixed formations was observed in oxidation at 1200 °C. These researchers mainly reduced the oxygen permeability of coatings by changing their chemical composition, reducing their porosity and preparing gradient coatings, thereby extending their service life.

To reduce the speed of oxygen reaching the metal bonding layer and solve the above problems to improve the performance of TBCs, an efficient method has been proposed as follows: We will prepare an ultra-thin zirconia layer on the surface of plasma-sprayed thermal barrier coatings via magnetron sputtering. The ultra-thin zirconia layer can not only prevent oxygen permeating the top ceramic, but can also reduce the direct contact between both corrosive environmental contaminants and stabilizers of zirconia. Plasma-sprayed coatings contain many small pores, and these pores may form continuous free channels in the coatings. If the ultra-thin zirconia layer can seal these pores, the surface thin layer will be a good barrier to oxygen and molten salts.

The partially yttrium-oxide-stabilized zirconia powder and coating have been previously prepared. $9.5\text{Y}_2\text{O}_3\text{-}5.6\text{Yb}_2\text{O}_3\text{-}5.2\text{Gd}_2\text{O}_3$ doped in ZrO_2 (YYG) was thought to have promising applications as a ceramic thermal barrier coating material in high-temperature environments due to its low thermal conductivity and high-temperature phase stability [24,25]. Its disadvantage is its poor thermal shock resistance. If the transmission rate of oxygen can be reduced, thereby reducing the oxidation rate of the bonding layer, this will greatly improve the service life and operation temperature of thermal barrier coatings and accelerate the development of aviation engines. This study mainly focuses on the effects of a thin layer of zirconia on the thermal properties of coatings, which hinders direct contacts between corrosive substances and the coating, reduces the oxygen transmission rate and improves the service life of high-temperature components in aviation engines and gas turbines.

2. Experimental Procedures

Powder prepared by the solid reaction method was used to prepare coatings, and then the thermal properties were tested.

2.1. Specimen Preparation

Powders were prepared by the solid reaction method. Firstly, oxides of Y_2O_3 (Aladdin, >99.9%), Yb_2O_3 (Aladdin, >99.9%), Gd_2O_3 (Aladdin, >99.9%) and ZrO_2 (Aladdin, >99.9%) were weighed according to the mass ratio of $9.5\text{Y}_2\text{O}_3\text{-}5.6\text{Yb}_2\text{O}_3\text{-}5.2\text{Gd}_2\text{O}_3\text{-}79.7\text{ZrO}_2$. All the oxides were mixed in absolute ethyl alcohol (Shandong Qilin Chemical Co., Ltd., Zibo, China, >99%) via high-energy ball milling at a speed of 400 r/min for 8 h, and then the mixture was dried in a drying box at 120 °C. Then, the mixture was placed in a high-temperature furnace and kept at 1500 °C for 8 h. Finally, the powder was used to prepare TBCs using an air plasma spray process, and the plasma spray parameters used are listed

in Table 1. The corrosion testing process was consistent with the literature [26,27]. The YSZ target (AECC Beijing Institute of Aeronautical Materials, Beijing, China, 99.99%) material was used for magnetron sputtering, and the power was 200 W.

Table 1. Plasma spray parameters used for spraying ceramic layer powders and bond layer powders.

Plasma Spray Parameters	Bond Layer	Ceramic Layer
Argon flow (NLPM)	45	45
Hydrogen flow (NLPM)	4.5	4.5
Amps (A)/volts (V)	420/50	620/62
Carrier gas flow (SCFH)	5	3
Powder feed rate (g/min)	26	26
Cooling air pressure (bar)	2.6	2.6
Spray distance (cm)	12	10.5
Gun speed (mm/s)	500	600

2.2. Structure Characterization and Property Measurement

Densities of the bulk samples were measured by Archimedes' method. XRD (PANalytical, Almelo, The Netherlands) using Cu Ka radiation ($k = 1.54 \text{ \AA}$) at 5 kV and 10 mA was performed to determine the phase compositions of synthesized samples over the range of $10\text{--}90^\circ$. General Structure Analysis System X'Pert High Score Plus 3.0 software was used to analyze the XRD patterns. Morphologies and chemical compositions were analyzed using a Cold Field Emission Scanning Electron Microscope (SEM, Hitachi SU8020, Tokyo, Japan) equipped with an energy-dispersive spectroscopy (EDS) unit. The thermal shock resistance was tested using a Muffle furnace. The samples were prepared on the surface of a superalloy with dimensions of $\phi 30 \times 5 \text{ mm}$ using the APS method. To examine the durability of the TBCs, a thermal cycling test was conducted at 1150°C in a chamber furnace in an atmospheric environment, which consisted of 4 min of heating up to 1150°C , 5 min resting at 1150°C and air-cooling to room temperature via a deionized water-cooling process. The properties of thermal insulation and the oxidation product on coatings were measured using an air plasma spray system (APS-3000, Beijing, China) at 1500°C , and the test details can be found in our previous work [28]. The actual thermal insulation ability was evaluated by the temperature difference between the substrate and ceramic.

3. Results and Discussion

3.1. XRD Analysis of Powders and Coatings

The YSZ and YYG XRD patterns of powders and coatings with and without an ultrathin dense layer are shown in Figure 1. The ceramic powders of YSZ and YYG have wide diffraction peaks, which might be attributed to the fine grains of the powders [29]. Some characteristic peaks of the tetragonal phase are present [30] at (101), (110), (112), etc., in the XRD patterns of the YYG powder. Figure 2 shows the X-ray diffraction patterns at high angle scans in the range of 2θ from 72.5° to 75.5° . It is obvious that the YYG coating with an ultrathin dense layer has characteristic peaks of both the YYG coating and YSZ coating at the same time, as shown in Figure 2(A,C). This proves that the dense layer is a tetragonal phase.

To further prove the phase constitution of coatings of YSZ and YYG, Figure 3 shows diagrams of the Raman shift of the coatings, respectively. The Raman signal from cubic zirconia is weaker than that from tetragonal zirconia; however, the sensitivity of the monoclinic phase in Raman spectroscopy is much higher than that in XRD [31,32]. The irreducible representation for optical and acoustical zone center phonons can be determined by a group theory analysis [33]. It can be observed that the Raman spectra of YSZ and YYG coatings contain the same peaks, which proves that they have the same phase structure. The YYG coating has broader Raman bands than those of the YSZ coating, especially around 615 cm^{-1} .

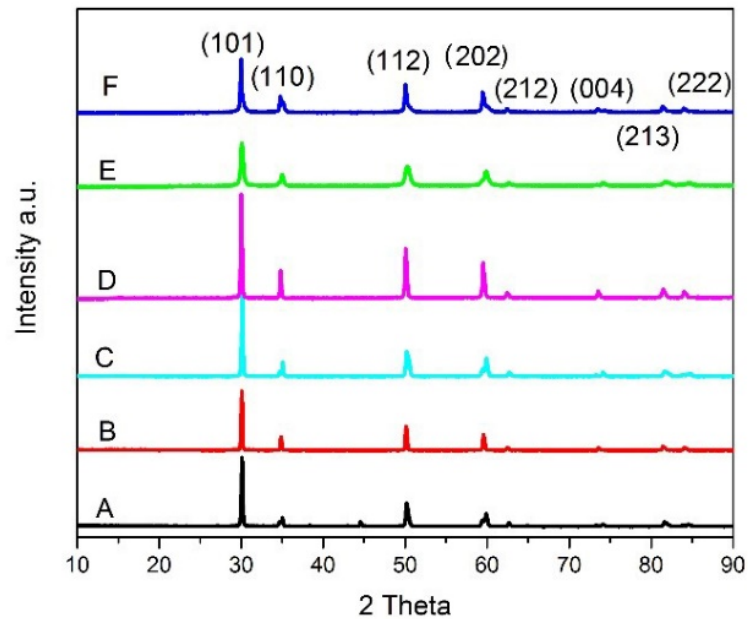


Figure 1. X-ray diffraction patterns of the YSZ powder (A), YYG powder (B), YSZ coating (C), YYG coating (D), YSZ coating with an ultrathin dense layer (E) and YYG coating with an ultrathin dense layer (F).

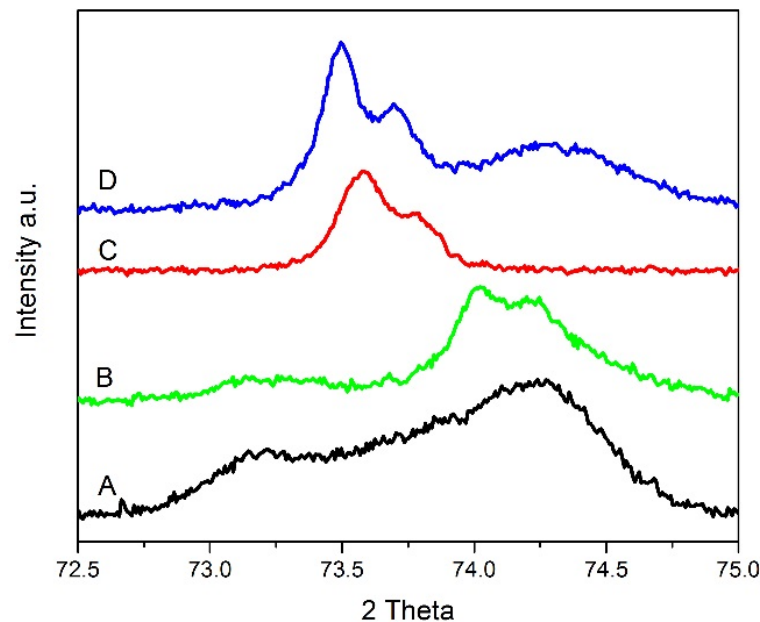


Figure 2. The X-ray diffraction patterns at high angle scans in the range of 2θ from 72.5° to 75.5° of YSZ powder (A), YSZ coating with ultrathin dense layer (B), YYG powder (C) and YYG coating with ultrathin dense layer (D).

3.2. Thermal Ablation Analysis

The thermal ablation experiment conditions are most similar to the real working conditions. Figure 4 shows typical surface photographs of the YYG coating with an ultrathin dense layer before ablation (a), after the first ablation (b) and after the second ablation (c) at 1500°C for 1000 s. After the first thermal ablation, the coating surface color changed from white to gray, but the coating did not fail. It is possible that the bond strength between the dense layer and the top layer is not sufficient to withstand the normal working environment at 1500°C . During the cooling process in the second thermal ablation experiment, the top layer of ceramic was partially removed, but the superalloy did not

fail. The coating protected the superalloy substrate well. The YYG coating without a dense layer failed after the first thermal ablation. Thus, the dense layer can prolong the working time of TBCs. Figure 5 shows the temperature distribution of the YYG coating during the thermal ablation process. The surface temperature of the top ceramics is around 1500 °C, and the back temperature of the superalloy is around 970 °C. The total thickness of the ceramic layer is around 1 mm, and the heat insulation is around 530 °C/mm. The heating rate and cooling rate of the ceramic coating surface are higher than those of the back of the superalloy. This is mainly because the specific heat capacity of the superalloy (712 J/(kg·°C)) is much higher than that of the ceramic coating (490 J/(kg·°C)) [34,35]. This mismatch in specific heat capacity may be one of the factors which leads to the failure of TBCs [36]. The superalloy and the ceramics are under the same conditions; thus, there will be a big difference in heating and cooling rates.

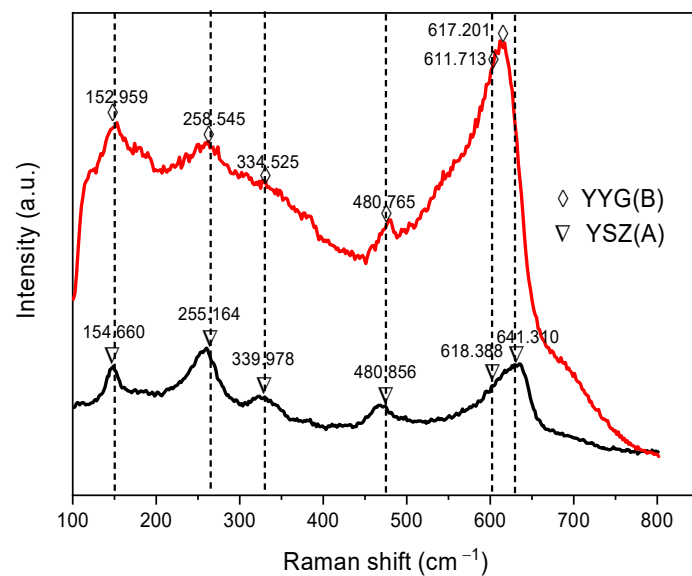


Figure 3. Raman spectra of the YSZ coating (A) and YYG coating (B).

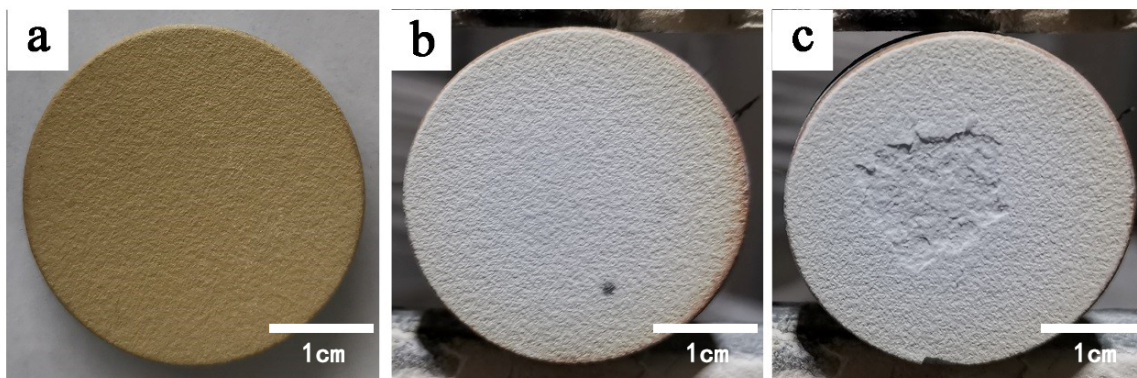


Figure 4. Typical surface photographs of the YYG coating with an ultrathin dense layer before ablation (a), after the first ablation (b) and after the second ablation (c) at 1500 °C for 1000 s.

Figure 6 shows the X-ray diffraction patterns of coatings after being kept at 1600 °C for 2 h and 8 h in a furnace. It is obvious that the relative peak strength of the ceramics decreases with an increase in the holding time at 1600 °C because the surface will be smoother and the coating will be denser after high-temperature treatment. This will decrease the scattering surface area. In addition, the heat transfer ability will be better at high temperatures. The relatively higher thermal conductivity will increase the failure rate of TBCs.

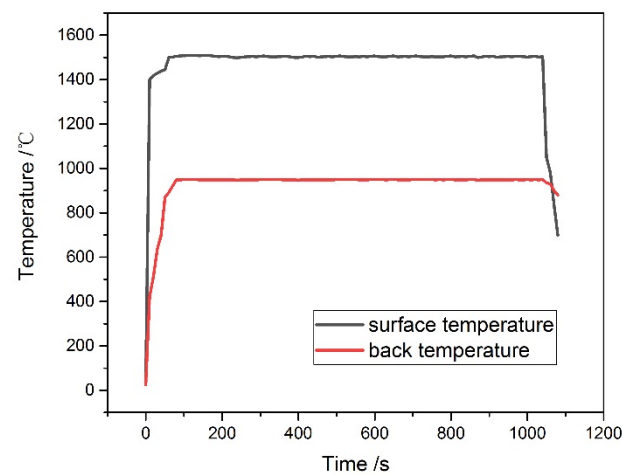


Figure 5. Heat insulation performance of the YYG coating with an ultrathin dense layer ablated at 1500 °C for 1000 s.

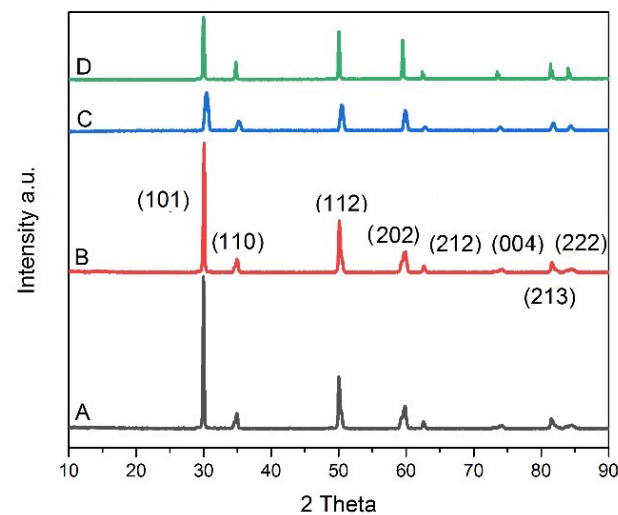


Figure 6. X-ray diffraction patterns of coatings after being kept at 1600 °C for 2 h (A is YSZ and B is YYG) and for 8 h (C is YSZ and D is YYG).

3.3. Corrosion Analysis

The working conditions of TBCs are extreme, and the salts and oxides in the air and fuel will react with the stabilizers of zirconium oxide. They will experience huge temperature differences in a short time. Different reactions will occur at different temperatures. Chemical reactions can increase the failure speed of TBCs. When the environmental temperature is around 900 °C, molten salts (V_2O_5 , Na_2SO_4 and $NaCl$) in the air can influence the lifetime of TBCs [37]. Molten salts were spun on the surface of the top ceramics and then maintained at 900 °C for 4 h. The corresponding elemental mapping results for the YYG coating with an ultrathin dense layer after hot corrosion tests in V_2O_5 - Na_2SO_4 - $NaCl$ molten salts at 900 °C for 4 h are shown in Figure 7. According to the elemental map of the intermixed zone, shown in Figure 7, Na, V, O and S elements were not uniformly distributed over the whole surface; S and O elements were distributed around V, which likely generates $NaVO_3$. The EDS spectrum of the YYG coating with an ultrathin dense layer (as shown in Figure 8) proved that there were no coating elements (such as Y, Yb, Gd) on the surface. The chemical compositions of the surface micrographs of the YYG coating with an ultrathin dense layer after corrosion (as shown in Table 2) show that the surface components are Na_2SO_4 and $NaVO_3$ [38]. This indicates that the surface of the ceramic layer of the thermal barrier coatings is completely covered in corrosive salts. No rare earth vanadate was found, indicating an enhanced corrosion resistance. The ultrathin dense layer can prevent molten

salts from reacting with the coatings, which is an efficient method to prolong the working time of TBCs.

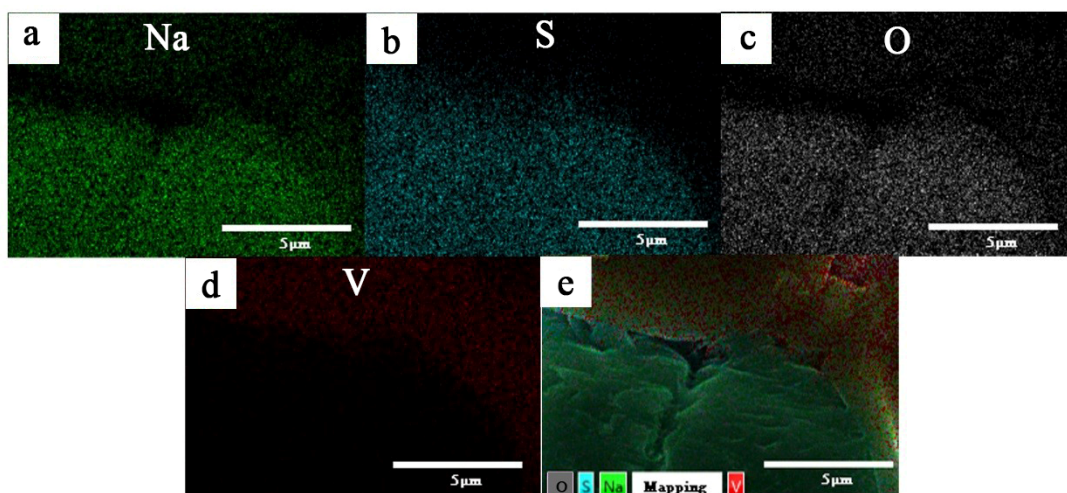


Figure 7. The corresponding elemental mapping results for the YYG coating with an ultrathin dense layer after hot corrosion tests in a $V_2O_5 + Na_2SO_4 + NaCl$ molten salt at $900\text{ }^\circ\text{C}$ for 4 h, (a) is Na, (b) is S, (c) is O, (d) is V, (e) is the combination of spectra.

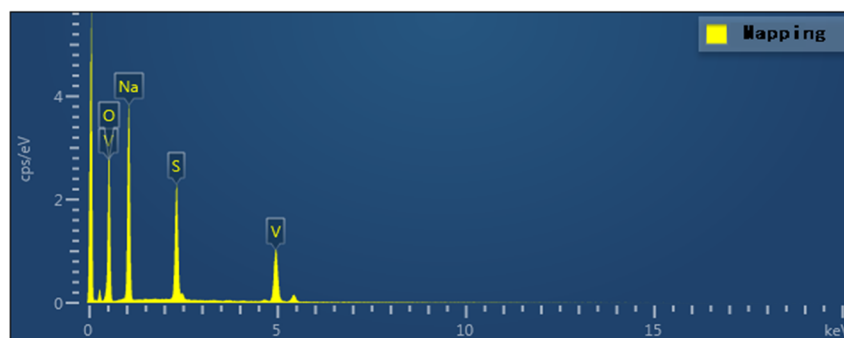


Figure 8. EDS spectrum of the YYG coating surface with an ultrathin dense layer after corrosion in a $V_2O_5 + Na_2SO_4 + NaCl$ molten salt at $900\text{ }^\circ\text{C}$ for 4 h.

Table 2. Chemical compositions of the surface micrographs of the YYG coating surface with an ultrathin dense layer after corrosion in a $V_2O_5 + Na_2SO_4 + NaCl$ molten salt at $900\text{ }^\circ\text{C}$ for 4 h.

Elements	O	Na	S	V
Mass ratio wt%	46.45	29.01	11.44	13.11
Atomic percentage	60.75	26.4	7.46	5.38

In the absence of any protection, the molten salt reacts with the stabilizers of zirconium oxide, resulting in the segregation failure of the coating [18,25,39]. According to previous low-temperature molten salt corrosion results, when a dense oxide film is prepared on the surface of the coating via the plasma spraying method, direct contact between the molten salt and the coating can be prevented, and the molten salt corrosion rate of the coating at about $900\text{ }^\circ\text{C}$ can be slowed down. Thus, we studied whether the dense oxide film can slow down the CMAS corrosion of the coating at $1400\text{ }^\circ\text{C}$. Figure 9 shows the surface element distribution of the coatings after the CMAS attack at $1400\text{ }^\circ\text{C}$ for 8 h determined by an EDS mapping test. The EDS result suggests (as shown in Figures 9 and 10) that CMAS has not reacted with the coating stabilizers. From Figure 9 and Table 3, it is obvious that CMAS has reacted with ZrO_2 at $1400\text{ }^\circ\text{C}$ [40], and only Ca, Mg, Al, Si, O and Zr were found on the surface, but elements such as Y, Yb, Gd were not detected, indicating that CMAS may

replace stabilizers and affect the service life of the coating. Figure 10 indicates that the surface of the ceramic layer of the thermal barrier coatings has been completely covered by CMAS. Oxide (CaO, MgO, Al₂O₃, SiO₂)-stabilized zirconia may form, indicating an enhanced corrosion resistance. Thus, CMAS will increase the failure rate of TBCs when the working temperature is higher than 1400 °C.

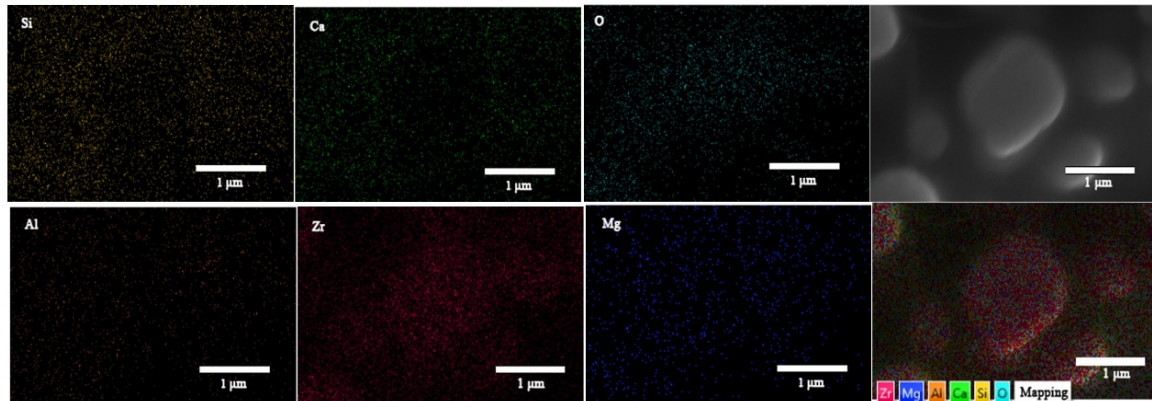


Figure 9. The surface microstructures and EDS mapping of the YYG coating with an ultrathin dense layer after corrosion by CMAS at 1400 °C.

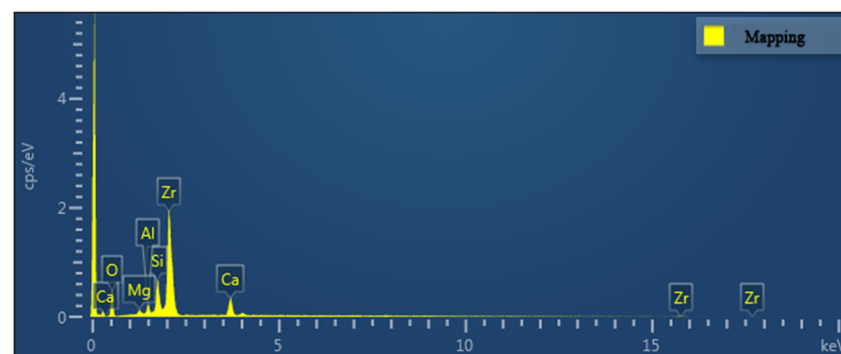


Figure 10. EDS spectrum of the YYG coating with an ultrathin dense layer surface after corrosion by CMAS at 1400 °C.

Table 3. Chemical compositions of the surface micrographs of the YYG coating surface with an ultrathin dense layer after corrosion by CMAS at 1400 °C.

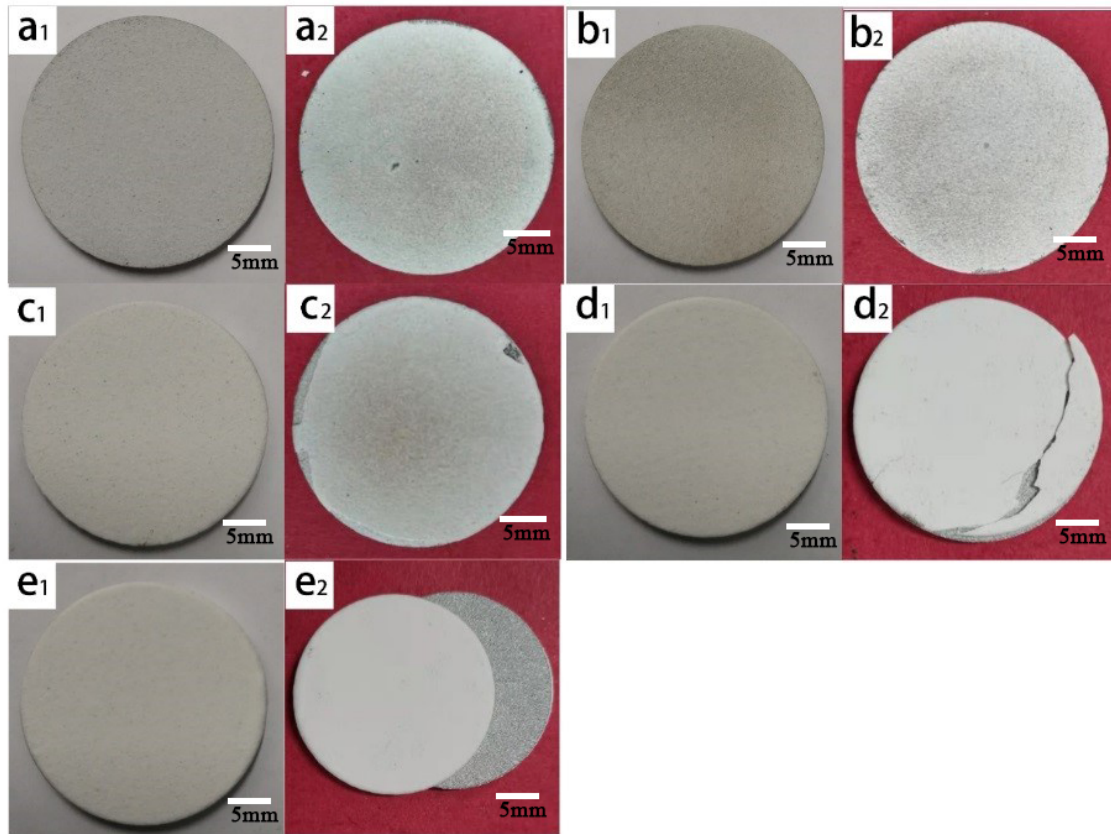
Elements	O	Mg	Al	Si	Ca	Zr
Mass ratio wt%	34.02	0.94	1.88	5.73	6.73	50.7
Atomic percentage	67.24	1.22	2.2	6.45	5.31	17.58

3.4. Thermal Shock Analysis

To closely imitate the real conditions, in the thermal cycling test, the coating was first cooled in air at least 6 times, and then cooled in deionized water at room temperature until failure. The thermal cycling test results of the YYG coatings with different thicknesses are shown in Table 4. It shows that the thermal cycles increase with a decrease in thickness; the finale failure photos are shown in Figure 11. It is clear that the top of the ceramic coating with a thickness of 900 μm is completely removed from the superalloy after two air cooling cycles, but the others are only removed partly. The test results show that the coating with an ultrathin dense layer can work normally when the thickness is no less than 300 μm, which is similar to the findings in [41].

Table 4. Thermal shock properties of the YYG coating with an ultrathin dense layer.

	50 μm	100 μm	300 μm	600 μm	900 μm
Air cooling cycles	6	6	6	6	2
Water cooling cycles	6	5	3	1	-

**Figure 11.** Thermal shock pictures of different-thickness YYG coatings at 1150 °C for 5 min: 50 μm (a), 100 μm (b), 300 μm (c), 600 μm (d), 900 μm (e). The subscript 1 represents before ablation, and the subscript 2 represents after ablation failure.

4. Conclusions

A YYG ceramic powder has been synthesized via the solid-state reaction method. Ceramic coatings with an ultrathin dense layer have been prepared via the air plasma spraying and magnetron sputtering methods. The insulation capacity of the thermal barrier coatings is nearly 530 °C/mm, which indicates that they can resist low-temperature molten salt ($\text{V}_2\text{O}_5 + \text{Na}_2\text{SO}_4 + \text{NaCl}$) corrosion and high-temperature CMAS corrosion and that they have a prolonged working time. The thermal shock resistance test shows that the coating with a sputtered ultrathin dense layer thickness of 300 μm performs twice as well as the coating without an ultrathin dense layer, demonstrating an improved thermal stability. The dense layer can slow down the oxidation rate of the metal bonding layer, extend the service life of the coating and greatly improve the workability of thermal barrier coatings. This can improve the service life of high-temperature components in aviation engines and gas turbines with different ceramic materials.

Author Contributions: Methodology, L.A., M.Y. and Y.Z.; Software, L.A., X.W. and Y.Z.; Validation, Y.L.; Investigation, L.A., M.Y. and Y.L.; Resources, Y.Z.; Data curation, X.W. and Y.L.; Writing—original draft, L.A. and X.W. All authors have read and agreed to the published version of the manuscript.

Funding: This research was funded by the Talent Introduction Project of Hubei Polytechnic University (No:21xjz12R) and the Scientific Research Project of Hubei Provincial Education Department (No: Q20224502).

Institutional Review Board Statement: Not applicable.

Informed Consent Statement: Not applicable.

Data Availability Statement: Data are contained within the article.

Conflicts of Interest: The authors declare no conflict of interest.

References

1. Zhou, F.; Wang, Y.; Liu, M.; Deng, C.; Zhang, X. Thermo-physical and thermal insulation properties of multi-scale nanostructured thermal barrier coatings using as-prepared t' -8YSZ feedstocks. *Ceram. Int.* **2019**, *45*, 24096–24103. [[CrossRef](#)]
2. Zhong, Y.; An, R.; Ma, H.; Wang, C. Low-temperature-solderable intermetallic nanoparticles for 3D printable flexible electronics. *Acta Mater.* **2019**, *162*, 163–175. [[CrossRef](#)]
3. Zhao, C.; Luo, L.; Lu, J.; Zhao, X.; Wang, X.; Guo, F.; Xiao, P. Investigation on the performance of air plasma sprayed thermal barrier coating with Lu/Hf-doped NiAl bond coat. *Surf. Coat. Technol.* **2019**, *360*, 140–152. [[CrossRef](#)]
4. Zhang, P.; Zhang, X.; Li, F.; Zhang, Z.; Wang, Y.; Li, H.; Ren, L.; Liu, M. Hot Corrosion Behavior of YSZ Thermal Barrier Coatings Modified by Laser Remelting and Al Deposition. *J. Therm. Spray Technol.* **2019**, *28*, 1225–1238. [[CrossRef](#)]
5. Zhang, H.; Liu, Z.; Yang, X.; Xie, H. Interface failure behavior of YSZ thermal barrier coatings during thermal shock. *J. Alloys Compd.* **2019**, *779*, 686–697. [[CrossRef](#)]
6. Yang, P.; Yang, D.; Hao, E.; An, Y.; Li, Y.; Wang, Z. Thermal shock resistance and failure analysis of $\text{La}_2(\text{Zr}_{0.75}\text{Ce}_{0.25})_2\text{O}_7$ -based TBCs produced by atmospheric plasma spraying. *Surf. Coat. Technol.* **2021**, *409*, 126903. [[CrossRef](#)]
7. Zhao, P.; Zhu, J.; Yang, K.; Li, M.; Shao, G.; Lu, H.; Ma, Z.; Wang, H.; He, J. Outstanding wear resistance of plasma sprayed high-entropy monoboride composite coating by inducing phase structural cooperative mechanism. *Appl. Surf. Sci.* **2023**, *616*, 156516. [[CrossRef](#)]
8. Yu, C.-T.; Xie, H.-Q.; Li, S.; Jiang, C.-Y.; Bao, Z.-B.; Zhang, W.; Zhang, L.; Pu, W.-Q.; Zhu, S.-L.; Wang, F.-H. Thermal cycling and interface bonding performance of single phase (Ni,Pt)Al coating with and without pure metastable tetragonal phase 4YSZ. *Appl. Surf. Sci.* **2023**, *615*, 156326. [[CrossRef](#)]
9. Yu, C.T.; Liu, H.; Zhang, J.; Ullah, A.; Bao, Z.B.; Jiang, C.Y.; Zhu, S.L.; Wang, F.H. Gradient thermal cycling behavior of a thermal barrier coating system constituted by NiCoCrAlY bond coat and pure metastable tetragonal nano-4YSZ top coat. *Ceram. Int.* **2019**, *45*, 15281–15289. [[CrossRef](#)]
10. Yang, L.; Zou, Z.; Kou, Z.; Chen, Y.; Zhao, G.; Zhao, X.; Guo, F.; Xiao, P. High temperature stress and its influence on surface rumpling in NiCoCrAlY bond coat. *Acta Mater.* **2017**, *139*, 122–137. [[CrossRef](#)]
11. Chen, L.; Wang, W.-J.; Li, J.-H.; Yang, G.-J. Suppressing the phase-transition-induced cracking of SiO_2 TGOs by lattice solid solution. *J. Eur. Ceram. Soc.* **2023**, *43*, 3201–3215. [[CrossRef](#)]
12. Wang, J.; Lu, X.; Hu, M.; Chen, M.; Wang, Y.; Shu, C.; Zhang, H.; Liu, B.; Sun, J.; Jing, Q. Phase stability, thermophysical properties, thermal shock behavior and CMAS resistance of Sc_2O_3 - CeO_2 co-stabilized ZrO_2 TBCs. *Surf. Coat. Technol.* **2023**, *467*, 129679. [[CrossRef](#)]
13. Wu, J.; Gao, Y.; Guo, C.; Guo, L. Laser surface modification to improve the resistance of CMAS + molten salt coupling corrosion to thermal barrier coatings. *Ceram. Int.* **2023**, *49*, 32282–32291. [[CrossRef](#)]
14. Krause, A.R.; Garces, H.F.; Dwivedi, G.; Ortiz, A.L.; Sampath, S.; Pature, N.P. Calcia-magnesia-alumino-silicate (CMAS)-induced degradation and failure of air plasma sprayed yttria-stabilized zirconia thermal barrier coatings. *Acta Mater.* **2016**, *105*, 355–366. [[CrossRef](#)]
15. Yao, Y.M.; Cai, J.; Gao, J.; Guan, Q.F.; Lyu, P.; Hua, Y.Q.; Ye, Y.X.; Xue, W. Thermal cycling behavior and stress distribution in TGO layer of MCrAlYX-type coatings via high-current pulsed electron beam modification. *Appl. Surf. Sci.* **2022**, *605*, 154674. [[CrossRef](#)]
16. Wei, Z.-Y.; Liu, Y.; Cheng, B.; Tahir, A. Influence of non-uniform feature of thermally grown oxide thickness on the local stress state and cracking behavior in TBC. *Surf. Coat. Technol.* **2022**, *443*, 128607. [[CrossRef](#)]
17. Li, B.; Chen, Z.; Zheng, H.; Li, G.; Li, H.; Peng, P. Wetting mechanism of CMAS melt on YSZ surface at high temperature: First-principles calculation. *Appl. Surf. Sci.* **2019**, *483*, 811–818. [[CrossRef](#)]
18. Vakili, H.; Ghasemi, R.; Rahimipour, M. Hot corrosion behaviour of plasma-sprayed functionally graded thermal barrier coatings in the presence of Na_2SO_4 + V_2O_5 molten salt. *Surf. Coat. Technol.* **2017**, *326*, 238–246. [[CrossRef](#)]
19. Shen, Z.; Liu, Z.; Huang, Z.; Mu, R.; He, L.; Liu, G. Thermal shock life and failure behaviors of $\text{La}_2\text{Zr}_2\text{O}_7$ /YSZ, $\text{La}_2\text{Ce}_2\text{O}_7$ /YSZ and $\text{Gd}_2\text{Zr}_2\text{O}_7$ /YSZ DCL TBCs by EB-PVD. *Mater. Charact.* **2021**, *173*, 110923. [[CrossRef](#)]
20. Wang, K.L.; Zhu, J.P.; Wang, H.L.; Yang, K.J.; Zhu, Y.M.; Qing, Y.B.; Ma, Z.; Gao, L.H.; Liu, Y.B.; Wei, S.H.; et al. Air plasma-sprayed high-entropy ($\text{Y}_{0.2}\text{Yb}_{0.2}\text{Lu}_{0.2}\text{Eu}_{0.2}\text{Er}_{0.2}$) $_3\text{Al}_5\text{O}_{12}$ coating with high thermal protection performance. *J. Adv. Ceram.* **2022**, *11*, 1571–1582. [[CrossRef](#)]

21. Tounsi, A.; Bousahla, A.A.; Tahir, S.I.; Mostefa, A.H.; Bourada, F.; Al-Osta, M.A.; Tounsi, A. Influences of different boundary conditions and Hygro-thermal environment on the free vibration responses of FGM sandwich plates resting on viscoelastic foundation. *Int. J. Struct. Stab. Dyn.* **2023**, 2450117. [[CrossRef](#)]
22. Naim Katea, S.; Riekehr, L.; Westin, G. Synthesis of nano-phase ZrC by carbothermal reduction using a ZrO₂-carbon nanocomposite. *J. Eur. Ceram. Soc.* **2021**, 41, 62–72. [[CrossRef](#)]
23. Doleker, K.M.; Ozgurluk, Y.; Karaoglanli, A.C. TGO growth and kinetic study of single and double layered TBC systems. *Surf. Coat. Technol.* **2021**, 415, 127135. [[CrossRef](#)]
24. Jung, S.-H.; Lu, Z.; Jung, Y.-G.; Song, D.; Paik, U.; Choi, B.; Kim, I.; Guo, X.; Zhang, J. Thermal durability and fracture behavior of layered Yb-Gd-Y-based thermal barrier coatings in thermal cyclic exposure. *Surf. Coat. Technol.* **2017**, 323, 39–48. [[CrossRef](#)]
25. Ejaz, N.; Ali, L.; Ahmed, F.; Awan, G.; Ghauri, K.M.; Nusair, A. Hot corrosion behavior of double ceramic layered CaZrO₃/Yttria-stabilized zirconia coatings. *Int. J. Appl. Ceram. Technol.* **2018**, 15, 53–62. [[CrossRef](#)]
26. Guo, L.; Yan, Z.; Yu, J.; Zhang, C.; Li, M.; Ye, F.; Ji, V. Hot corrosion behavior of TiO₂ doped, Yb₂O₃ stabilized zirconia exposed to V₂O₅+ Na₂SO₄ molten salt at 700–1000 °C. *Ceram. Int.* **2018**, 44, 261–268. [[CrossRef](#)]
27. Cui, J.-J.; Ouyang, J.-H.; Liu, Z.-G. Hot corrosion behavior of LaMgAl₁₁O₁₉ ceramic coated with molten CMAS deposits at temperature of 1250 °C in air. *J. Alloys Compd.* **2016**, 685, 316–321. [[CrossRef](#)]
28. Yang, M.; Zhu, Y.; Wang, X.; Wang, Q.; Ai, L.; Zhao, L.; Chu, Y. A novel low thermal conductivity thermal barrier coating at super high temperature. *Appl. Surf. Sci.* **2019**, 497, 143774. [[CrossRef](#)]
29. Guo, L.; Zhang, Y.; Ye, F.; White, M.A. Phase Structure Evolution and Thermo-Physical Properties of Nonstoichiometry Nd_{2-x}Zr_{2+x}O_{7+x/2} Pyrochlore Ceramics. *J. Am. Ceram. Soc.* **2015**, 98, 1013–1018. [[CrossRef](#)]
30. Loghman-Estarki, M.R.; Shoja Razavi, R.; Edris, H.; Bakhshi, S.R.; Nejati, M.; Jamali, H. Comparison of hot corrosion behavior of nanostructured ScYSZ and YSZ thermal barrier coatings. *Ceram. Int.* **2016**, 42, 7432–7439. [[CrossRef](#)]
31. Li, M.; Cheng, Y.; Guo, L.; Zhang, C.; Zhang, Y.; He, S.; Ye, F. Preparation of plasma sprayed nanostructured GdPO₄ thermal barrier coating and its hot corrosion behavior in molten salts. *Ceram. Int.* **2017**, 43, 7797–7803. [[CrossRef](#)]
32. Lughì, V.; Clarke, D.R. Transformation of Electron-Beam Physical Vapor-Deposited 8 wt% Yttria-Stabilized Zirconia Thermal Barrier Coatings. *J. Am. Ceram. Soc.* **2005**, 88, 2552–2558. [[CrossRef](#)]
33. Bouvier, P.; Gupta, H.C.; Lucazeau, G. Zone center phonon frequencies in tetragonal zirconia: Lattice dynamical study and new assignment proposition. *J. Phys. Chem. Solids* **2001**, 62, 873–879. [[CrossRef](#)]
34. Han, M.; Huang, J.; Chen, S. A parametric study of the Double-Ceramic-Layer Thermal Barrier Coating Part II: Optimization selection of mechanical parameters of the inside ceramic layer based on the effect on the stress distribution. *Surf. Coat. Technol.* **2014**, 238, 93–117. [[CrossRef](#)]
35. Han, M.; Zhou, G.; Huang, J.; Chen, S. A parametric study of the double-ceramic-layer thermal barrier coatings part I: Optimization design of the ceramic layer thickness ratio based on the finite element analysis of thermal insulation (take LZ₇C₃/8YSZ/NiCoAlY DCL-TBC for an example). *Surf. Coat. Technol.* **2013**, 236, 500–509. [[CrossRef](#)]
36. Chen, X.; Sun, Y.; Hu, J.; Li, J.; Deng, C.; Wu, D.; Zeng, D.; Li, W.; Liu, Y.; Zou, B.; et al. Thermal cycling failure of the multilayer thermal barrier coatings based on LaMgAl₁₁O₁₉/YSZ. *J. Eur. Ceram. Soc.* **2020**, 40, 1424–1432. [[CrossRef](#)]
37. Tabeshfar, M.; Salehi, M.; Dini, G.; Dahl, P.I.; Einarsrud, M.-A.; Wiik, K. Hot corrosion of Gd₂Zr₂O₇, Gd₂Zr₂O₇/YbSZ, YSZ + Gd₂Zr₂O₇/YbSZ, and YSZ thermal barrier coatings exposed to Na₂SO₄ + V₂O₅. *Surf. Coat. Technol.* **2021**, 409, 126718. [[CrossRef](#)]
38. Guo, L.; Zhang, C.; He, Q.; Yu, J.; Yan, Z.; Ye, F.; Dan, C.; Ji, V. Microstructure evolution and hot corrosion mechanisms of Ba₂REAlO₅ (RE = Yb, Er, Dy) exposed to V₂O₅+ Na₂SO₄ molten salt. *J. Eur. Ceram. Soc.* **2018**, 38, 3555–3563. [[CrossRef](#)]
39. Chang, J.X.; Wang, D.; Zhang, G.; Lou, L.H.; Zhang, J. Interaction of Ta and Cr on Type-I hot corrosion resistance of single crystal Ni-base superalloys. *Corros. Sci.* **2017**, 117, 35–42. [[CrossRef](#)]
40. Kang, Y.X.; Bai, Y.; Fan, W.; Yuan, T.; Gao, Y.; Bao, C.G.; Li, B.Q. Thermal cycling performance of La₂Ce₂O₇/50 vol.% YSZ composite thermal barrier coating with CMAS corrosion. *J. Eur. Ceram. Soc.* **2018**, 38, 2851–2862. [[CrossRef](#)]
41. Wang, Z.; Liu, T.; Wang, E.; Hu, S.; Xie, Z.; Gong, X. Effect of Al plating on growth behavior of TGO layer in CoCrNiAlY-YSZ-RSZ dual-ceramic coating. *Surf. Coat. Technol.* **2022**, 432, 128060. [[CrossRef](#)]

Disclaimer/Publisher's Note: The statements, opinions and data contained in all publications are solely those of the individual author(s) and contributor(s) and not of MDPI and/or the editor(s). MDPI and/or the editor(s) disclaim responsibility for any injury to people or property resulting from any ideas, methods, instructions or products referred to in the content.